J Physiol 595.19 (2017) pp 6349–6362

The Journal of Physiology

Distinct temporal filters in mitral cells and external tufted cells of the olfactory bulb

Christopher E. Vaaga[1,2] and Gary L. Westbrook[1]

[1] *Vollum Institute, Oregon Health and Science University, Portland, OR, USA*
[2] *Neuroscience Graduate Program, Oregon Health and Science University, Portland, OR, USA*

Key points

- The release probability of the odorant receptor neuron (ORN) is reportedly one of the highest in the brain and is predicted to impose a transient temporal filter on postsynaptic cells.
- Mitral cells responded to high frequency ORN stimulation with sustained transmission, whereas external tufted cells responded transiently.
- The release probability of ORNs (0.7) was equivalent across mitral and external tufted cells and could be explained by a single pool of slowly recycling vesicles.
- The sustained response in mitral cells resulted from dendrodendritic amplification in mitral cells, which was blocked by NMDA and mGluR1 receptor antagonists, converting mitral cell responses to transient response profiles.
- Our results suggest that although the afferent ORN synapse shows strong synaptic depression, dendrodendritic circuitry in mitral cells produces robust amplification of brief afferent input, and thus the relative strength of axodendritic and dendrodendritic input determines the post-synaptic response profile.

Abstract Short-term synaptic plasticity is a critical regulator of neural circuits, and largely determines how information is temporally processed. In the olfactory bulb, afferent olfactory receptor neurons respond to increasing concentrations of odorants with barrages of action potentials, and their terminals have an extraordinarily high release probability. These features suggest that during naturalistic stimuli, afferent input to the olfactory bulb is subject to strong synaptic depression, presumably truncating the postsynaptic response to afferent stimuli. To examine this issue, we used single glomerular stimulation in mouse olfactory bulb slices to measure the synaptic dynamics of afferent-evoked input at physiological stimulus frequencies. In cell-attached recordings, mitral cells responded to high frequency stimulation with sustained responses, whereas external tufted cells responded transiently. Consistent with previous reports, olfactory nerve terminals onto both cell types had a high release probability (0.7), from a single pool of slowly recycling vesicles, indicating that the distinct responses of mitral and external tufted cells to high frequency stimulation did not originate presyaptically. Rather, distinct temporal response profiles in mitral cells and external tufted cells could be attributed to slow dendrodendritic responses in mitral cells, as blocking this slow current in mitral cells converted mitral cell responses to a transient response profile, typical of external tufted cells. Our results suggest that despite strong axodendritic synaptic depression, the balance of axodendritic and

The manuscript was first published as a preprint: Vaaga CE and Westbrook GL (2017). Distinct temporal filters in mitral cells and external tufted cells of the olfactory bulb. bioRxiv https://doi.org/10.1101/135541

DOI: 10.1113/JP274608

dendrodendritic circuitry in external tufted cells and mitral cells, respectively, tunes the postsynaptic responses to high frequency, naturalistic stimulation.

(Received 8 May 2017; accepted after revision 2 August 2017; first published online 8 August 2017)
Corresponding author C. E. Vaaga: Neurobiology Department, Northwestern University, 2220 Campus Drive, Evanston, IL, 60208, USA. Email: Christopher.vaaga@northwestern.edu

Abbreviation ORN, odorant receptor neuron.

Introduction

The computational capacity of neural circuits is largely determined by the short-term synaptic dynamics within the circuit (Abbott & Regehr, 2004), as determined by pre- and postsynaptic mechanisms. Short-term synaptic depression, which generally occurs at high release probability synapses, results in a net decrease in postsynaptic responses with repeated stimulation, and is often attributed to depletion of the readily releasable pool of synaptic vesicles (Liley & North, 1953; Betz, 1970; von Gersdorff & Borst, 2002; Regehr, 2012). However, at some synapses, multiple pools of synaptic vesicles with distinct release probabilities can protect the circuit from synaptic depression during high frequency stimulation (Lu & Trussell, 2016; Taschenberger *et al.* 2016; Turecek *et al.* 2016).

In the olfactory bulb, principal neurons receive monosynaptic input from olfactory receptor neuron afferents (Gire & Schoppa, 2009; Najac *et al.* 2011; Gire *et al.* 2012; Vaaga & Westbrook, 2016). Odorant receptor neurons (ORNs) respond to increasing odorant concentrations with monotonic increases in firing frequency up to 100 Hz (Sicard, 1986; Duchamp-Viret *et al.* 1999; Rospars *et al.* 2003; Tan *et al.* 2010). Furthermore, the release probability of the afferent synapse between the ORN and its postsynaptic targets is one of the highest reported in the brain (*ca* 0.8–0.9; Murphy *et al.* 2004). Together, these features suggest that the transmission between ORNs and principal neurons is subject to robust short-term depression. However, *in vivo*, mitral cells respond to olfactory input with sustained responses (Giraudet *et al.* 2002; Nagayama *et al.* 2004; Leng *et al.* 2014), suggesting either that release probability during trains is not as high as has been reported, or that other circuit mechanisms maintain sustained transmission.

To examine the synaptic dynamics between ORN afferents and principal neurons in response to physiologically relevant stimulation frequencies, we recorded the postsynaptic responses of mitral cells and external tufted cells during high frequency afferent stimulation. Our results suggest that the high release probability and slow vesicle dynamics within the ORN are optimized for faithful transmission, but dendrodendritic amplification in mitral cells compensates for the strong synaptic depression and strongly amplifies afferent input.

Methods

Animals

We used adult (> p24) male and female C57Bl6/J as well as Tg(Thy1-YFP) GJrs heterozygous mice. The Oregon Health and Science University Institutional Animal Care and Use Committee approved all animal procedures.

Slice preparation

Olfactory bulb slices were prepared as described previously (Schoppa & Westbrook, 2001). Mice were given an intraperitoneal injection of 2% 2,2,2-tribromoethanol (0.7–0.8 ml) and monitored until fully anaesthetized, then transcardially perfused with oxygenated 4°C modified artificial cerebrospinal fluid (ACSF), which contained (in mM): 83 NaCl, 2.5 KCl, 1 NaH_2PO_4, 26.2 $NaHCO_3$, 22 dextrose, 72 sucrose, 0.5 $CaCl_2$, 3.3 $MgSO_4$ (300–310 mosmol l^{-1}, pH 7.3). The brain was quickly removed and coronally blocked at the level of the striatum. Horizontal sections (300 μm) through the olfactory bulb were made using a Leica 1200S vibrating blade microtome. Slices were recovered in warm (32–36°C) ACSF for 30 min and then were stored at room temperature until transfer to the recording chamber. Unless otherwise noted, the ACSF contained (in mM): 125 NaCl, 25 $NaHCO_3$, 1.25 NaH_2PO_4, 3 KCl, 2.5 dextrose, 2 $CaCl_2$, 1 $MgCl_2$ (300–310 mosmol l^{-1}, pH 7.3).

Electrophysiology

Whole cell voltage clamp and current clamp recordings were made from mitral cells and external tufted cells under differential interference contrast (DIC) optics. Mitral cells and external tufted cells were identified as described previously (Hayar *et al.* 2005; Vaaga & Westbrook, 2016). Briefly, mitral cells were identified by their soma position within the mitral cell layer and external tufted cells were identified by their relatively large soma positioned within the outer two-thirds of the glomerular layer. Patch pipettes (3–5 MΩ) contained (in mM): 120 potassium gluconate, 20 KCl, 10 HEPES, 0.1 EGTA, 4 Mg-ATP, 0.3 Na-GTP, 0.05 Alexa-594 hydrazide and 5 QX-314. We made no correction for the liquid junction potential (−7 mV). During cell-attached recordings, the membrane patch was held at −70 mV after achieving a gigaohm seal. Data were

acquired using a Multiclamp 700b amplifier (Molecular Devices, Sunnyvale, CA, USA) and AxographX acquisition software. Data were digitized at 10 kHz and low pass Bessel filtered at 4 kHz. For cell-attached recordings, the data were filtered *post hoc* at 1 kHz. During whole-cell recordings the series resistance was continually monitored with a −10 mV hyperpolarizing step. Series resistance was generally < 25 MΩ and was not compensated. Cells with greater than 30% change in series resistance during the recording were excluded from analysis. All recordings were made at 34-36°C.

EPSCs were elicited using single glomerulus theta stimulation, as described previously (Vaaga & Westbrook, 2016). Stimulation was provided by a constant current stimulator (100 μs, 3.2–32 mA) in conjunction with a small bore theta electrode (2 μm) placed directly in the axon bundle entering the target glomerulus. All recordings were made along the medial aspect of the olfactory bulb, and recordings were only made if the ORN bundle entering the target glomerulus was clearly identifiable under DIC optics. Stimulation trains (10, 25 and 50 Hz, 20 pulses) were chosen to represent the approximate firing rate of ORNs in response to odorant presentation (Sicard, 1986; Duchamp-Viret *et al.* 1999; Carey *et al.* 2009; Tan *et al.* 2010). ORN stimulation was repeated at 60 s intervals, to prevent rundown. All drugs were prepared from stock solutions according to manufacturer specifications and applied via a gravity fed perfusion system. The drugs used included 2 mM kynurenic acid, 500 nM sulpiride, 200 nM CGP55845, 10 μM 3-((R)-2-carboxypiperazin-4-yl)-propyl-1-phosphonic acid (CPP) and 20 μM CPCCOEt. All drugs were purchased from Abcam Biochemical (Cambridge, MA, USA) or Tocris Biosciences (Ellisville, MO, USA).

Data analysis

Electrophysiology data were analysed using AxographX (www.axograph.com) and IGOR Pro (version 6.22A, Wavemetrics, Lake Oswego, OR, USA). Spike waveforms in cell-attached recordings were detected using a threshold detection criterion in AxographX, which was used to calculate the total spike number and to generate raster plots. Voltage clamp traces represent the average of 5–10 sweeps after baseline subtraction. Fast EPSC amplitude measurements were made foot-to-peak, to eliminate any contribution of the slow current. To directly measure the slow current we recorded the EPSC amplitude just prior to each stimulus within the train. The total charge transfer (0–2.5 s after stimulus onset) was measured using a built-in AxographX routine. Data were normalized to the first fast peak EPSC amplitude, unless otherwise noted.

To estimate release probability, we used two methods to calculate the size of the readily releasable pool, each of which utilizes different assumptions (Neher, 2015; Thanawala & Regehr, 2016). In the Schneggenburger, Meyer and Neher (SMN) method, the cumulative fast EPSC amplitude (at 50 Hz stimulation) was plotted as a function of stimulus number and a linear fit was made using the last five responses in the train. The readily releasable pool size was estimated as the y-intercept of the linear fit (Schneggenburger *et al.* 1999, 2002), and release probability was calculated by dividing the initial EPSC amplitude by the size of the readily releasable pool. In the Elmqvist–Quastal (EQ) method (Elmqvist & Quastel, 1965), the fast EPSC amplitude was plotted as a function of the cumulative EPSC amplitude. A linear fit to the first three EPSCs was used to calculate the size of the readily releasable pool (x-intercept). Release probability was then calculated as in the SMN method.

Statistics

All data are reported as means ± SEM unless otherwise indicated. Statistical analysis was performed in Prism6 (GraphPad Software, La Jolla, CA, USA). One-way and two-way repeated measure experiments were analysed using ANOVA with Holm–Sidak *post hoc* pairwise comparisons as indicated in the text. To compare the exponential fit across data sets, an extra sum of squares F test was performed to compare lines of best fit. In agreement with previous electrophysiological studies, data were assumed to be normally distributed, and were thus analysed using parametric statistics. Student's t test for paired or unpaired data was used as appropriate. Sample sizes were chosen to detect an effect size of 20%, based on prior, similar experiments, with a power of 0.8. In all experiments, the initial value for α was set to $P < 0.05$, and was adjusted for multiple comparisons as appropriate.

Results

Different temporal response profiles in mitral and external tufted cells

To examine the synaptic dynamics of principal neuron activity in response to high frequency afferent stimulation, we first measured the spiking of mitral and external tufted cells using cell-attached recordings. Both cell types responded to 50 Hz ORN stimulation with spikes throughout the stimulus train (Fig. 1*A*–*D*). Mitral cells and external tufted cells produced similar numbers of spikes early in the train; however, action potentials in external tufted cells gradually decreased, such that by the seventh stimulus, mitral cells produced more action potentials per successive stimulus than external tufted cells (two-way ANOVA; $P < 0.01$; $n = 7$ mitral cells, 8 external tufted cells; Fig. 1*E*). Likewise, mitral cells continued to spike well after the end of the stimulus train, contributing to the higher total number of spikes produced (mitral

cells: 161.8 ± 27.2 spikes per trial, $n = 7$ cells; external tufted cells: 45.2 ± 9.0 spikes per trial, $n = 8$ cells; 2.5 s window, unpaired Student's t test: $P = 0.009$; Fig. 1*F*). In fact, in mitral cells, 87.1 ± 15.3 spikes were produced after the stimulus ($n = 7$ cells), whereas only 9.2 ± 3.6 spikes were produced after the stimulus in external tufted cells (2 s window; $n = 7$ cells; unpaired Student's t test: $P = 0.003$). Similar response patterns were observed when the ORN was stimulated with shorter, high frequency bursts (5 pulses at 50 Hz), which may more accurately represent the time course of ORN firing *in vivo* (Carey & Wachowiak, 2011). In response to short bursts, mitral cells produced 80.1 ± 18.1 spikes ($n = 7$ cells) whereas external tufted cells produced 17.6 ± 6.0 spikes ($n = 7$ cells; unpaired Student's t test: $P = 0.007$). Furthermore, mitral cells produced significantly more spikes after the stimulus train (mitral cells: 56.3 ± 13.8 spikes after the train, $n = 7$ cells; external tufted cells: 9.7 ± 4.6 spikes after the train; unpaired Student's t test: $P = 0.008$), consistent with the sustained firing of mitral cells.

In order to quantify the temporal filter in mitral cells and external tufted cells, we calculated the percentage of the total spikes that occurred within 20 ms of each stimulus in the 50 Hz train. Using this metric, a steep input–output curve is indicative of a transient temporal filter. In both mitral cells and external tufted cells, the input–output curve was fit by a single exponential decay. In mitral cells, this relationship was relatively shallow ($\tau = 5.2$ stimuli),

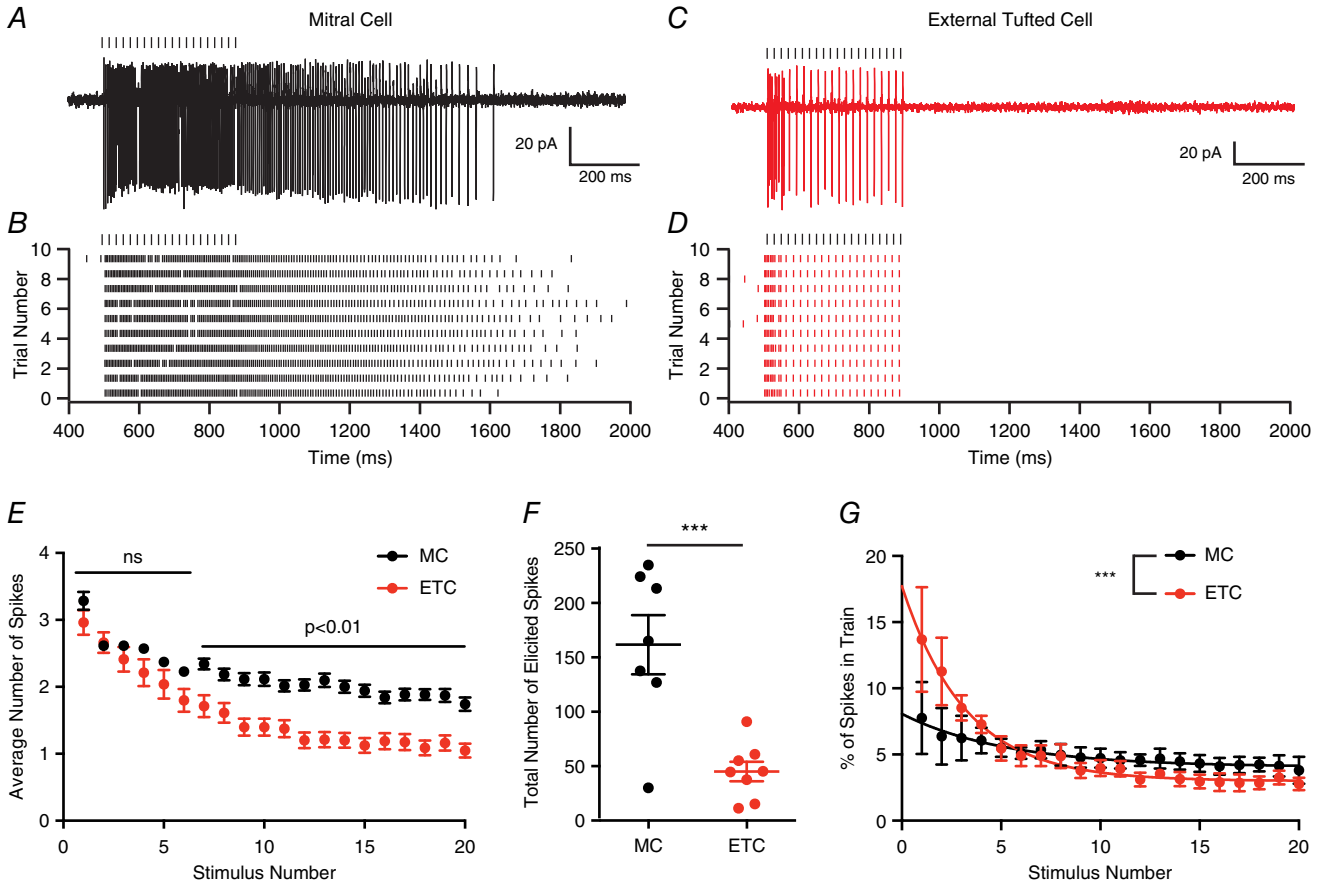

Figure 1. Sustained transmission in mitral and external tufted cells
A, cell attached recording from mitral cell in response to 50 Hz ORN stimulation. *B*, raster plot of mitral cell response. Mitral cells responded to ORN stimulation with sustained responses, which outlasted the stimulus. *C* and *D*, cell attached recording (*C*) and associated raster plot (*D*) of external tufted cell response to 50 Hz ORN stimulation. External tufted cells produced much more transient response profiles. *E*, plot of the average number of action potentials produced following each stimulus in the train. Mitral cells and external tufted cells produce similar numbers of action potentials at the beginning of the train. By the end of the train, however, mitral cells produce approximately twice as many action potentials as external tufted cells. *F*, the total number of spikes produced (within 2.5 s) in mitral cells is significantly higher than in external tufted cells. *G*, plot of the fraction of total spikes in the train as a function of stimulus number. Mitral cells have a more shallow relationship, consistent with sustained transmission. External tufted cells have a significantly steeper relationship, indicative of transient response profiles. [Colour figure can be viewed at wileyonlinelibrary.com]

consistent with the observed sustained transmission. On average, mitral cells produced 7.8 ± 2.7% of total spikes immediately after the first stimulus and 3.8 ± 1.0% of spikes following the final stimulus ($n = 7$ cells). In contrast, external tufted cells had a much steeper input–output relationship ($\tau = 3.2$ stimuli), producing 13.7 ± 4.0% of total spikes after the first stimulus and 2.8 ± 0.47% following the final stimulus (extra sum of squares F test: $P < 0.0001$, $n = 8$ cells). Thus the two cell types have distinct response properties with mitral cells responding to high frequency stimulation with a sustained response, whereas external tufted cells respond transiently.

Despite the distinct temporal responses across the stimulus train, the relative timing of spikes elicited at the beginning of the stimulus was remarkably stereotyped between mitral cells and external tufted cells. There was no difference in the first spike latency (mitral cells: 3.7 ± 1.07 ms, $n = 7$ cells; external tufted cells: 3.4 ± 0.90 ms, $n = 8$ cells; unpaired Student's t test: $P = 0.83$), consistent with monosynaptic afferent input (Vaaga & Westbrook, 2016). Furthermore, the standard deviation (jitter) of each successive spike elicited within the first 20 ms of the stimulus was not significantly different for the first four spikes (1st spike: external tufted cell: 0.6 ± 0.4 ms, mitral cell: 0.6 ± 0.3 ms, $P = 0.98$; 2nd spike: external tufted cell: 0.9 ± 0.2 ms, mitral cell: 1.0 ± 0.2 ms, $P = 0.72$; 3rd spike: external tufted cell: 1.0 ± 0.3 ms; mitral cell: 1.4 ± 0.3 ms, $P = 0.36$; 4th spike: external tufted cell: 0.8 ± 0.2 ms; mitral cell: 1.7 ± 0.6 ms, $P = 0.25$; $n = 7$ mitral cells, 8 external tufted cells, unpaired Student's t test).

Responses to repeated high frequency stimulation

Although mitral cells and external tufted cells have distinct temporal response profiles to single bursts of high frequency stimulation, we also wanted to examine the responses of both cells to repeated high frequency bursts, which more accurately mimic active sniffing events. It is possible that the sustained response of mitral cells makes them less effective at following high frequency stimulation. To test this, we stimulated the ORN at 50 Hz (5 pulses), repeating the stimulation 5 times with an inter-burst interval of 200 ms, representing an approximate sniff frequency of 5 Hz (Welker, 1964; Youngentob *et al.* 1987). In mitral cells, repeated high frequency stimulation elicited a sustained barrage of action potentials that persisted throughout the stimulus train and beyond (6 of 7 cells; Fig. 2*A* and *B*). In addition to the sustained spiking response, the majority of cells (5 of 7 cell) also had transient increases in firing rate associated with each high frequency ORN burst (45.9 ± 4.4% of total spikes during ORN bursts; $n = 7$ cells; Fig. 2*A* and *B*), indicating that mitral cells are, in fact, well positioned to follow repeated stimulation. Conversely, in external tufted cells, spiking was phase locked to ORN stimulation, with little sustained spiking (85.6 ± 7.8% of total spikes during ORN bursts; $n = 7$ cells; unpaired Student's t test: $P = 0.0008$; Fig. 2*C* and *D*). In some cells (3 of 7) phase locked responses were limited to the first two ORN bursts. Together these data indicate that in response to repeated high frequency stimulation, both cell types have transient ORN-driven responses, but mitral cells have additional sustained spiking between each ORN burst.

High release probability from a single pool of synaptic vesicles

Differences in release probability of ORN terminals could underlie the distinct responses of mitral cells and external tufted cells, as release probability has only been examined in tufted cells (Murphy *et al.* 2004). To determine the release probability, we stimulated at high frequencies to estimate the size of the readily releasable pool using two analytical approaches as described in Methods (Elmqvist & Quastel, 1965; Schneggenburger *et al.* 1999; Neher, 2015; Thanawala & Regehr, 2016). Consistent with a high release probability synapse, 50 Hz trains of stimuli elicited robust depression of the phasic EPSC amplitude in mitral cells (Fig. 3*A*) and external tufted cells (Fig. 3*B*). Both the SMN method (Fig. 3*C*, *E*) and EQ method (Fig. 3*D*, *E*) yielded similar estimates of the size of the readily releasable pool in mitral cells and external tufted cells. Accordingly, there was no difference in the release probability between cell types (SMN: mitral cells: 0.67 ± 0.02, $n = 7$ cells, external tufted cells: 0.71 ± 0.06, $n = 8$ cells, $P = 0.51$; EQ: mitral cells: 0.66 ± 0.02, external tufted cells: 0.73 ± 0.03, $P = 0.14$; Fig. 3*E*). These results indicate that the release probability of ORNs is high, but somewhat lower than previous estimates in tufted cells (Murphy *et al.* 2004), which likely reflects the activation of presynaptic D_2 and $GABA_B$ receptors in our experiments (Nickell *et al.* 1994; Aroniadou-Anderjaska *et al.* 2000; Ennis *et al.* 2001; Wachowiak *et al.* 2005; Maher & Westbrook, 2008; Shao *et al.* 2009; Vaaga *et al.* 2017). Consistent with this hypothesis, measurements of the release probability in D_2 and $GABA_B$ receptor antagonists (500 nM sulpiride and 200 nM CGP55845, respectively) increased the release probability to 0.95 ± 0.06 (SMN method, $n = 4$ cells, unpaired Student's t test: $P = 0.008$). Furthermore, 2 mM kynurenic acid, which blocks receptor saturation and desensitization (Trussell *et al.* 1993; Wadiche & Jahr, 2001; Foster *et al.* 2002; Wong *et al.* 2003; Chanda & Xu-Friedman, 2010) did not affect the paired pulse ratio (control: 0.24 ± 0.05; 2 mM kynurenic acid: 0.25 ± 0.05, $n = 5$ cells, paired Student's t test: 0.70; Fig. 3*F* and *G*), suggesting that at the ORN afferent synapse, synaptic depression is primarily mediated by presynaptic factors, and is consistent with univesicular release (Murphy *et al.* 2004; Taschenberger *et al.* 2016).

In other circuits (Mennerick & Matthews, 1996; Sakaba & Neher, 2001; Lu & Trussell, 2016; Turecek *et al.* 2016), multiple pools of synaptic vesicles have heterogeneous release probabilities, which, if present, could obscure our measurements of release probability and support sustained transmission at high stimulation frequencies (Neher, 2015; Turecek *et al.* 2016). To test for the presence of multiple pools of synaptic vesicles, we stimulated at 10 Hz (20 pulses) to deplete the high release probability pool then switched to 50 Hz stimulation (20 pulses), a protocol that has been used to reveal a transient facilitation resulting from the low release probability of a separate pool of vesicles (Lu & Trussell, 2016; Turecek *et al.* 2016). In both mitral cells and external tufted cells this stimulation protocol failed to elicit facilitation (Fig. 4*A* and *B*); rather, switching to high frequency stimulation elicited further depression of the ORN-evoked phasic EPSC (external tufted cell: $EPSC_{21}$: 25.3 ± 0.4% of control, $EPSC_{22}$: 14.7 ± 0.2% of control, $n = 7$ cells; mitral cell: $EPSC_{21}$: 14.7 ± 1.6% of control, $EPSC_{22}$: 8.5 ± 1.4% of control, $n = 4$ cells; Fig. 4*B*), suggesting a single pool of synaptic vesicles in both cells. Likewise, the decay of the phasic EPSC amplitude as a function of stimulus number was best fit with a single exponential function in both cell types (external tufted cell: τ: 0.68; extra sum of squares F test: $P = 0.49$; mitral cell: τ: 0.78; extra sum of squares F test: $P = 0.18$; Fig. 4*C*). Together, these data indicate that a single pool of high release probability vesicles is sufficient to explain release from afferent olfactory nerve terminals.

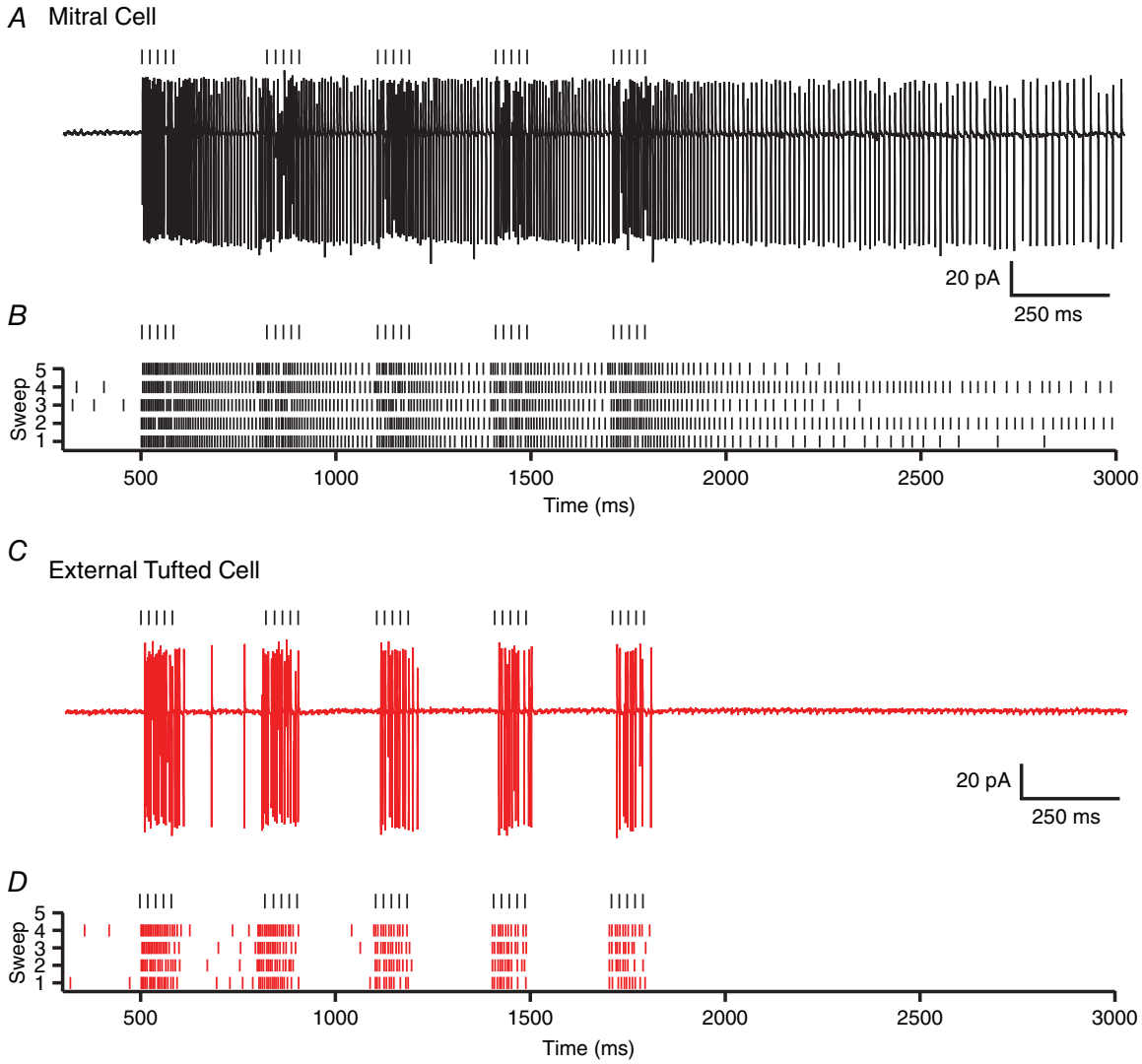

Figure 2. Distinct temporal responses to repeated high frequency stimulation
A, cell attached recording from a mitral cell in response to repeated high frequency stimulation mimicking active sniffing. *B*, raster plot of mitral cell spiking response showing both transient and sustained responses to repeated high frequency stimulation. *C*, cell attached recording from an external tufted cell. *D*, raster plot demonstrating transient response profile of external tufted cells. [Colour figure can be viewed at wileyonlinelibrary.com]

Sustained responses in some cases can be maintained despite high release probability as a result of fast vesicle replenishment (Wang & Kaczmarek, 1998; Saviane & Silver, 2006). However, the phasic EPSC amplitude recovered surprisingly slowly, following a double exponential time course (data pooled from both cell types; τ_1: 0.79 s; τ_2: 8.23 s; Fig. 4*D*–*F*), suggesting that fast vesicle replenishment does not contribute to the sustained responses in mitral cells.

Dendrodendritic excitation maintains sustained transmission

Our results suggest that properties of the afferent presynaptic terminal alone cannot explain the sustained transmission observed in mitral cells. To determine what mechanisms support sustained transmission, we examined the responses of mitral cells and external tufted cells in voltage clamp following stimulation across a range of stimulus frequencies (10 Hz, 25 Hz, 50 Hz; Fig. 5*A* and

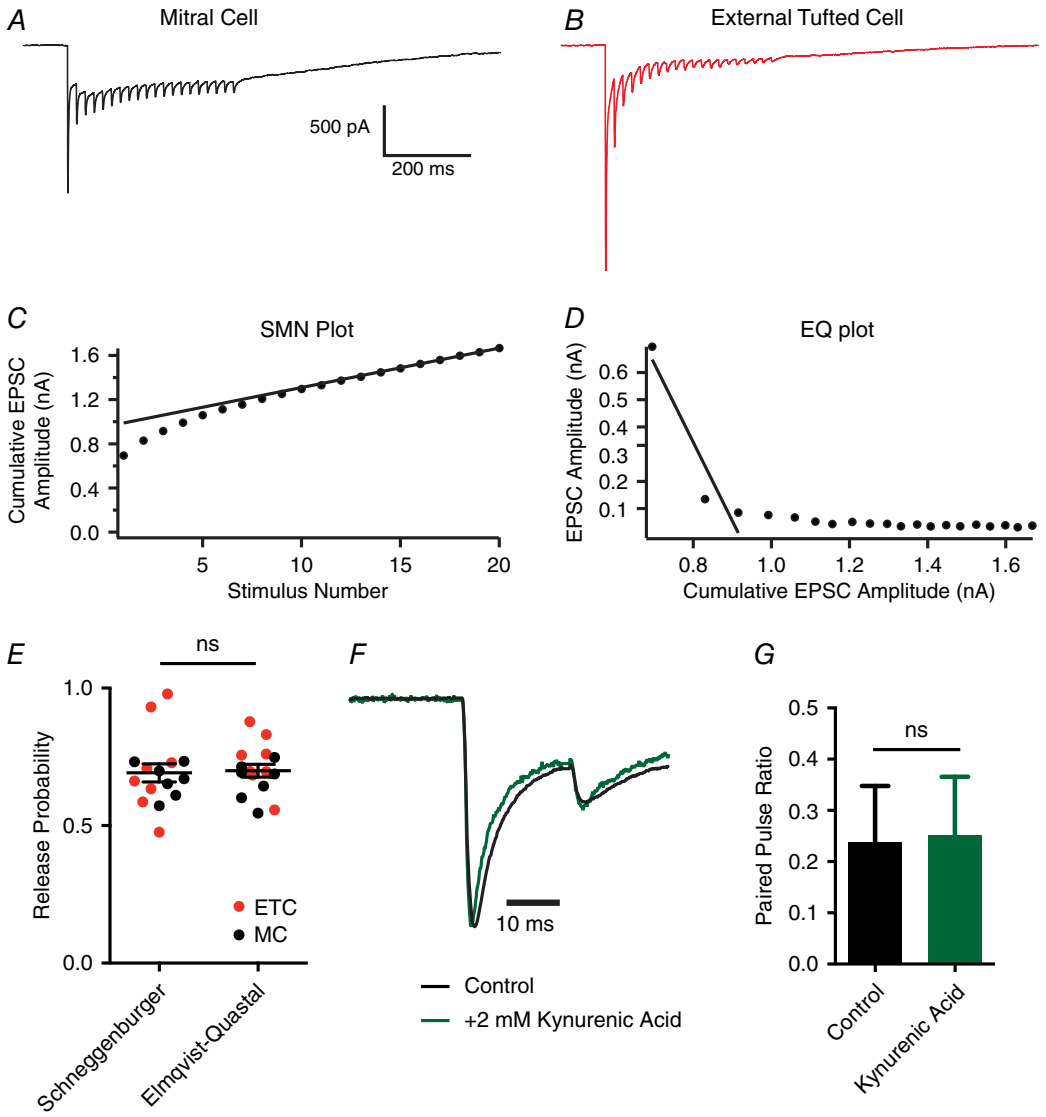

Figure 3. Olfactory receptor neurons have a high release probability
A and *B*, representative whole-cell voltage clamp responses to 50 Hz stimulation in mitral cells (*A*) and external tufted cells (*B*). *C* and *D*, estimate of the release probability using the SMN method (*C*) and EQ method (*D*) for the mitral cell shown in *A*. *E*, estimates of release probability do not differ between the SMN and EQ methods, and there was no difference in the release probability between mitral cells and external tufted cells. *F*, paired pulse ratio in external tufted cells before and after addition of 2 mM Kynurenic acid to prevent receptor saturation and desensitization. The response in Kynurenic acid has been scaled to the control. *G*, summary of the paired pulse ratio in external tufted cell before and after 2 mM Kynurenic acid, suggesting postsynaptic saturation and desensitization do not contribute to synaptic depression. [Colour figure can be viewed at wileyonlinelibrary.com]

B). Across stimulus frequencies, the phasic EPSC showed robust depression (Fig. 5*D* and *E*). Surprisingly, even relatively low stimulus frequencies (10 Hz) elicited strong depression in mitral and external tufted cells, consistent with the slow vesicle replenishment rates and unusually high release probability. In both cell types, there was a significant effect of stimulus frequency on the degree of phasic EPSC depression (one-way ANOVA: mitral cell: $P = 0.0003$; external tufted cell: $P < 0.0001$). In both cells, the depression increased from 10 Hz to 25 Hz (mitral cells: 10 Hz: 16.4 ± 1.3% of $EPSC_1$, $n = 6$ cells; 25 Hz: 9.4 ± 2.1% of $EPSC_1$ $n = 5$ cells, Holm–Sidak *post hoc* comparison: $P < 0.05$; external tufted cells: 10 Hz: 14.8 ± 2.0, $n = 7$ cells; 25 Hz: 5.8 ± 0.9% of control, $n = 7$ cells, Holm–Sidak *post hoc* comparison: $P < 0.001$), but was not significantly different between 25 Hz and 50 Hz (mitral cell: 25 Hz: 9.4 ± 2.1% of $EPSC_1$ $n = 5$ cells, 50 Hz: 5.4 ± 0.9% of $EPSC_1$, $n = 6$ cells, Holm–Sidak *post hoc* comparison: $P > 0.05$; external tufted cell: 25 Hz: 5.8 ± 0.9% of $EPSC_1$, $n = 7$ cells, 50 Hz: 4.4 ± 0.6% of $EPSC_1$, $n = 8$ cells, Holm–Sidak *post hoc* comparison: $P > 0.05$). There was no difference in the total degree of phasic depression between mitral cells and external tufted cells at any stimulus frequency tested (Fig. 5*G*), consistent with similar presynaptic properties of the incoming afferents.

However in mitral cells, phasic EPSCs were superimposed on a large, slow envelope current at all stimulus frequencies, reflecting the much larger dendrodendritic currents in mitral cells compared to external tufted cells (Fig. 5*C*; Vaaga & Westbrook, 2016). In mitral cells, the decay kinetics, but not the rising phase, of the fast EPSC became slightly slower during high frequency stimulation (data not shown), likely reflecting AMPA receptor-dependent dendrodendritic glutamate release (Fig. 5*A*). Such kinetic changes in the EPSC decay were not observed in external tufted cells (Fig. 5*B*), consistent with the lack of secondary dendrodendritic activation in external tufted cells (Vaaga and Westbrook, 2016). The total charge transfer was nearly 3 times larger in mitral cells (10 Hz: mitral cell: 219.9 ± 50.6 pC, $n = 6$ cells, external tufted cell: 84.4 ± 23.25 pC, $n = 6$ cells, Holm–Sidak *post hoc* comparison: $P < 0.05$; 25 Hz: mitral cell: 268.0 ± 43.4 pC, $n = 5$ cells, external tufted cell: 75.5 ± 24.7 pC, $n = 7$ cells, Holm–Sidak *post hoc* comparison: $P < 0.01$; 50 Hz: mitral cell: 309.9 ± 50.1 pC, $n = 7$ cells, external tufted cell: 78.3 ± 12.3 pC, $n = 7$ cells; Holm–Sidak *post hoc* comparison: $P < 0.001$; Fig. 5*F*). Interestingly, the charge transfer was not sensitive to stimulation frequency (mitral cell: one-way ANOVA: $P = 0.43$; external tufted cell: one-way ANOVA: $P = 0.96$; Fig. 5*F*), consistent with an all-or-none dendrodendritic slow EPSC (Carlson *et al.* 2000; De Saint Jan *et al.* 2009; Gire & Schoppa, 2009). Unlike the phasic responses, the degree of depression of the slow envelope current within the stimulus train was significantly different between mitral cells and external tufted cells (10 Hz: mitral cell:

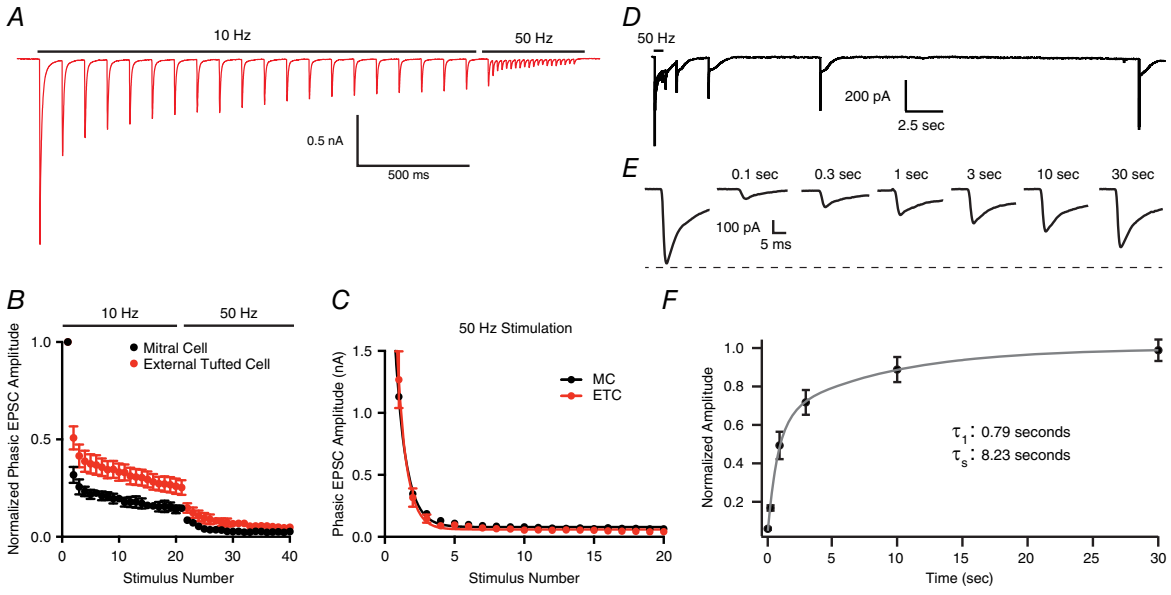

Figure 4. Single pool of slowly recycling vesicles
A, representative external tufted cell recording showing 10 Hz stimulation followed by 50 Hz stimulation. *B*, group data showing immediate depression following 10 Hz stimulation, suggesting a single pool of synaptic vesicles in both mitral cells and external tufted cells. *C*, in both cell types, the phasic EPSC amplitude plotted as a function of stimulus number is fit by a single exponential decay. *D* and *E*, recovery of phasic EPSC amplitude following 50 Hz stimulation suggests that vesicle replenishment is slow. *F*, recovery time course (pooled data from both mitral and external tufted cells) is best fit by a double exponential. [Colour figure can be viewed at wileyonlinelibrary.com]

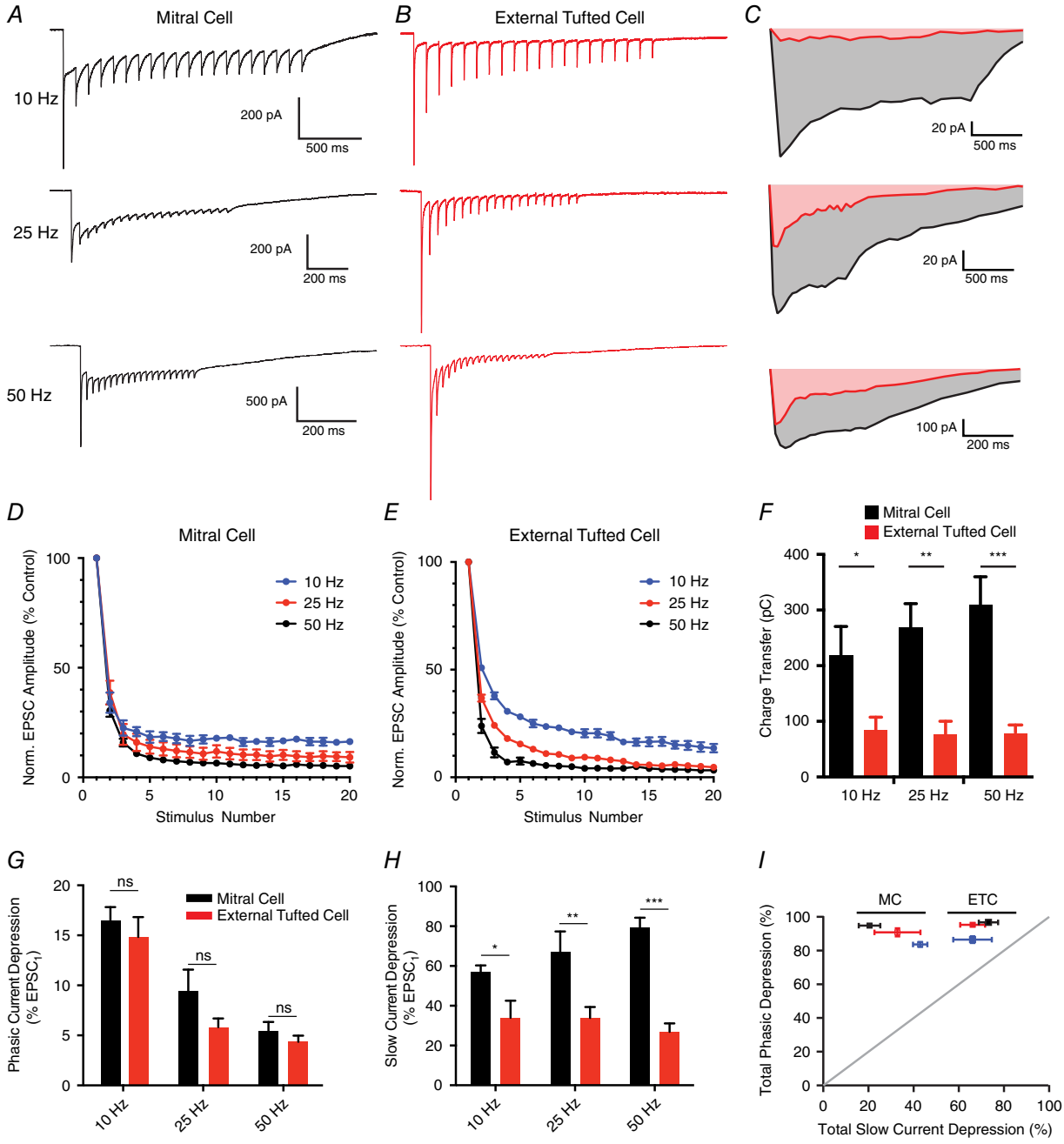

Figure 5. Differential modulation of phasic and slow currents in mitral and external tufted cells
A and *B*, whole-cell voltage clamp responses of mitral cells (*A*) and external tufted cells (*B*) to stimulation at various frequencies (10, 25, 50 Hz). *C*, comparison of the slow, envelope current measured in mitral cells and external tufted cells at each stimulus frequency. Mitral cells had consistently larger envelope currents. *D*, depression of the phasic EPSC amplitude as a function of stimulus number in mitral cells across stimulation frequencies (10 Hz, 25 Hz, 50 Hz). *E*, depression of phasic EPSC amplitude as a function of stimulus number in external tufted cells. *F*, the total charge transfer (measured 2.5 s after stimulus onset) was significantly larger in mitral cells than external tufted cells across all stimulation frequencies. There was no significant difference across stimulus frequencies within either cell type. *G*, total phasic depression in mitral cells and external tufted cells across stimulation frequencies. There was no significant difference between cell types at any frequency tested. *H*, total slow current depression in mitral cells and external tufted cells across stimulation frequencies. Mitral cells had significantly less slow current depression at all stimulus frequencies tested. *I*, plot showing a direct comparison of phasic depression and tonic depression across cell types and frequencies (10 Hz, 25 Hz, 50 Hz). Although the phasic depression was similar between cell types and frequencies, the slow current was differentially regulated in mitral cells and external tufted cells. [Colour figure can be viewed at wileyonlinelibrary.com]

57.1 ± 3.2% of $EPSC_1$, external tufted cell 34.0 ± 8.4% of $EPSC_1$, Holm–Sidak *post hoc* comparison: $P < 0.05$; 25 Hz: mitral cell: 67.2 ± 10.2% of $EPSC_1$, external tufted cell: 33.9 ± 5.5% of $EPSC_1$, Holm–Sidak *post hoc* comparison: $P < 0.01$; 50 Hz: mitral cell: 79.5 ± 4.8% of $EPSC_1$, external tufted cell: 26.8 ± 4% of $EPSC_1$, Holm–Sidak *post hoc* comparison: $P < 0.0001$; Fig. 5*H*).

In both mitral cells and external tufted cells, the depression of the phasic component was significantly larger than the depression of the slow, envelope current, and therefore all the data points fell above the unity line in a plot of phasic EPSC depression as a function of slow EPSC depression (Fig. 5*I*). Furthermore, the similarity of phasic depression and distinct slow current depression across cell types produced two identifiable clusters when the phasic and slow current depression were directly compared (Fig. 5*I*). Together these data suggest that a robust slow current supports sustained transmission in mitral cells, which is relatively insensitive to short-term depression and stimulus frequency.

The mitral cell slow current is responsible for sustained transmission

To explicitly test the role of the slow current in generating the sustained transmission in mitral cells, we blocked NMDA and mGluR1 receptors (10 μM CPP and 20 μM CPCCOEt, respectively), which effectively blocks the slow current in mitral cells (De Saint Jan & Westbrook, 2007; Vaaga & Westbrook, 2016). As expected, bath application of NMDA and mGluR1 antagonists reduced the total charge transfer in mitral cells (mitral cell: 309.9 ± 50.1 pC, $n = 7$ cells; mitral cell + CPP/CPCCOEt: 42.3 ± 8.5 pC, $n = 6$ cells, Holm–Sidak *post hoc* comparison: $P < 0.0001$; Fig. 6*A* and *B*), to levels comparable to the charge transfer in external tufted cells (external tufted cell: 78.27 ± 12.26, $n = 7$ cells, Holm–Sidak *post hoc* comparison: $P > 0.05$; Fig. 6*B*). Thus, blocking the slow current converts the mitral cell response pattern to an external tufted cell pattern.

In cell attached recordings of mitral cells, blocking NMDA and mGluR1 receptors also caused a 4-fold reduction in the total number of spikes produced following 50 Hz stimulation (mitral cell: 161.8 ± 27.2 spikes, $n = 7$ cells; mitral cell + CPP/CPCCOEt: 37.62 ± 7.3 spikes, $n = 5$ cells, Holm–Sidak *post hoc* comparison: $P < 0.001$; external tufted cell: 45.2 ± 9.0 spikes, $n = 8$ cells; Holm–Sidak *post hoc* comparison: $P > 0.05$; Fig. 6*D*). Furthermore, bath application of NMDA and mGluR1 receptor antagonists also altered the temporal patterning of spikes, converting the sustained responses of mitral cells to more transient responses (extra sum of squares *F* test: $P < 0.001$; Fig. 6*E*), which were not significantly different from the responses in external tufted cells (extra sum of squares *F* test: $P > 0.05$; Fig. 6*F*). Together these data suggest that differences in the amplitude of the slow current between mitral cells and external tufted cells are responsible for the sustained transmission in mitral cells, and produce their distinct temporal spiking patterns.

Discussion

In the glomerular microcircuit, the interplay of axodendritic and dendrodendritic synapses is critical to postsynaptic processing of afferent input. Although the primary function of the glomerulus is to enhance the signal-to-noise ratio (Chen & Shepherd, 2005), the synaptic dynamics in response to high frequency ORN stimulation have not previously been examined. Here we demonstrate that mitral cells and external tufted cells respond to high frequency afferent input with distinct temporal filters. Mitral cells produce sustained responses, requiring dendrodendritic amplification, whereas the lack of dendrodendritic amplification in external tufted cells results in transient responses. During repeated high frequency stimulation, which mimics active sniffing, mitral cell responses contained both a sustained and phase-locked component, whereas external tufted cell responses were primarily phase-locked. Together, our results indicate that axodendritic and dendrodendritic circuits are functionally separable such that the relative balance of the two circuits determines the temporal filter of the postsynaptic cell.

Comparison with other synapses

Previous steady state measurements of ORN release probability were near 1 (Murphy *et al.* 2004). Our results using high frequency trains of stimuli match those estimates when presynaptic D_2 and $GABA_B$ receptors are blocked. However, tonic and/or afferent-evoked activation of presynaptic D_2 and $GABA_B$ receptors during high frequency trains reduced the release probability by approximately 30%. Although many synapses, such as the climbing fibre synapse in the cerebellum, have a high release probability (Silver *et al.* 1998; Dittman *et al.* 2000), such terminals generally show multi-vesicular release (Wadiche & Jahr, 2001; Rudolph *et al.* 2015). However, the similar paired pulse ratio in control and low affinity antagonists suggest that ORN synapses operate using univesicular release (Murphy *et al.* 2004; Taschenberger *et al.* 2016). Although a uniquantal, high release probability synapse occurs in barrel cortex between layer 4 and layer 2/3 neurons (Silver *et al.* 2003), the presynaptic neuron generally fires only one to two action potentials in response to whisker stimulation *in vivo* (Brecht & Sakmann, 2002). Thus synaptic depression resulting from a high release probability is unlikely to impact the postsynaptic response. The univesicular, high release probability of the ORN, therefore, is

unusual because individual ORNs sustain firing at high frequencies (*ca* 50 Hz) in response to odorants (Sicard, 1986; Duchamp-Viret *et al.* 1999; Carey *et al.* 2009; Tan *et al.* 2010).

To maintain transmission under these conditions, the high initial release probability of the ORN could be compensated by fast vesicle recycling (Kushmerick *et al.* 2006; Saviane & Silver, 2006) or a second pool of low release probability vesicles (Lu & Trussell, 2016; Taschenberger *et al.* 2016; Turecek *et al.* 2016). These properties, however, are not present in ORNs. In fact, the recovery of the fast EPSC following depletion was approximately 10-fold slower than at the calyx of Held (Kushmerick *et al.* 2006), suggesting that individual ORNs may only transiently contribute to the postsynaptic response, thereby providing a rationale for the massive convergence of unimodal ORNs onto single glomeruli.

Distinct roles of axodendritic and dendrodendritic input

One advantage of such a high initial release probability is that odorant binding events in the periphery are faithfully transmitted to the olfactory bulb in a nearly

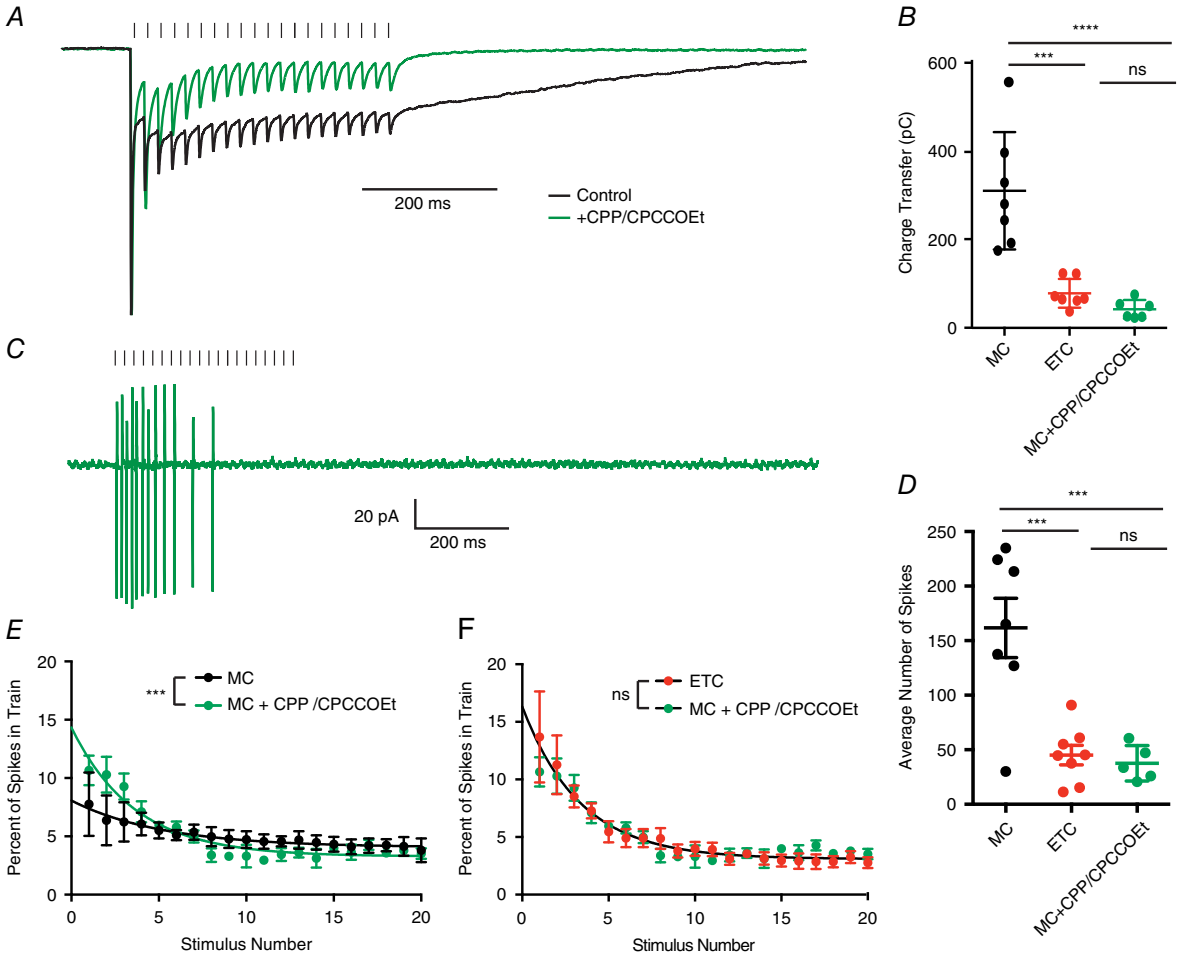

Figure 6. Blocking the slow current converts mitral cell responses into external tufted cell responses
A, peak scaled comparison of the whole cell voltage clamp recordings from mitral cells in control and 10 μM CPP/20 μM CPCCOEt in response to 50 Hz ORN stimulation. As expected, CPP/CPCCOEt blocked a significant portion of the slow envelope current. *B*, comparison of the total charge transfer in mitral cells, external tufted cells and mitral cells with CPP/CPCCOEt shows that blocking the NMDA/mGluR1 receptor-dependent current significantly reduces the total charge transfer to levels comparable to external tufted cells. *C*, cell-attached recording from mitral cell in response to 50 Hz ORN stimulation shows transient spiking profile of mitral cells when NMDA and mGluR1 receptors are blocked. *D*, the total number of action potentials produced in mitral cells with NMDA and mGluR1 receptors are similar to external tufted cell responses. *E*, comparison of the temporal profile of mitral cell spiking in control and with CPP/CPCCOEt. Block of NMDA and mGluR1 receptors reveals transient response profile of mitral cells. *F*, with NMDA and mGluR1 receptors blocked, the temporal profile of mitral cell spiking is not significantly different from the responses of external tufted cells. [Colour figure can be viewed at wileyonlinelibrary.com]

all-or-none manner. The olfactory system is exquisitely sensitive, capable of detecting odorants at concentrations as low as 1 part per 10^{15} molecules (Julius & Katz, 2004). In the periphery, this high sensitivity is achieved through biochemical amplification downstream of G-protein-coupled odorant receptors, such that a single odorant receptor-binding event can elicit an action potential in the ORN (Lynch & Barry, 1989). The high release probability of ORNs maintains the high sensitivity of the olfactory system, by ensuring that ORN activity is faithfully converted to a postsynaptic response. However, this circuit design comes at a cost in that individual nerve terminals can only transiently contribute to postsynaptic activation, thereby requiring an ensemble of functionally redundant channels to accurately convey information with high fidelity.

However, the high release probability of axodendritic input comes at a cost: the 'noisy' olfactory environment dramatically increases the total number of activated glomeruli in response to ambient air. Thus, multiple mechanisms, including dendrodendritic amplification, boost the signal-to-noise ratio within the glomerulus (Carlson *et al.* 2000; Chen & Shepherd, 2005; De Saint Jan & Westbrook, 2007; Vaaga & Westbrook, 2016). Our results demonstrate that the robust increase in synaptic charge associated with the slow dendrodendritic current, selectively expressed in mitral cells, effectively converts the transient axodendritic input into a sustained response.

Our results indicate that both mitral cells and external tufted cells are capable of following repeated ORN stimulations, which mimic active sniff frequencies (Welker, 1964; Youngentob *et al.* 1987). These data are consistent with *in vivo* recordings from mitral cells, which show distinct ORN-evoked transients during active sniffing (Carey & Wachowiak, 2011). In our experiments, mitral cells and external tufted cells differ in the sustained firing rate during high frequency stimulation, as external tufted cell responses were primarily phase locked to ORN stimulation. These results suggest that in response to active sniffing, mitral cells and external tufted cells convey temporally distinct information, resulting from different degrees of dendrodendritic amplification.

Parallel input paths convey temporally distinct information

Mitral and external tufted cells represent parallel input pathways. For example, *in vivo*, tufted cells respond to lower odorant concentrations, have concentration-invariant responses, and respond to odorants earlier in the sniff cycle (Nagayama *et al.* 2004; Fukunaga *et al.* 2012; Igarashi *et al.* 2012; Kikuta *et al.* 2013). Mitral cells, on the other hand, are more narrowly tuned than tufted cells, and shift their responses relative to the sniff cycle in response to increasing odorant concentrations (Nagayama *et al.* 2004; Kikuta *et al.* 2013). These *in vivo* results are consistent with the view that tufted cell responses maintain the sensitivity of the ORN, via strong afferent-evoked responses. On the other hand, mitral cells, while still responsive to stimuli at sniff frequencies as shown in our experiments, provide robust amplification, via strong dendrodendritic circuitry.

Within piriform cortex, the concentration-invariant network of activated pyramidal cells encodes odorant identity whereas concentration is encoded by the temporal response profiles of pyramidal cells (Bolding & Franks, 2017). The spiking patterns of these pyramidal cells have two distinct peaks, one with a short latency and one with a longer latency. As concentration increases, the lag between these peaks shortens (Bolding & Franks, 2017). Mechanistically, this may result from the integration of olfactory bulb projection neurons with distinct temporal spiking profiles. Such an activation scheme would require overlapping projection patterns in piriform cortex, but single axon tracing studies suggest that mitral cells and tufted cells project to largely non-overlapping regions of olfactory cortex (Igarahsi *et al.* 2012). Resolving the exact projection patterns and mechanisms behind generating distinct timing signals in piriform cortex is critical to understanding the encoding of concentration within the olfactory system. Our results, however, demonstrate that the balance of axodendritic and dendrodendritic synaptic strength likely contributes to the unique computations within these parallel input pathways, by imposing unique temporal filters in each cell type.

References

Abbott LF & Regehr WG (2004). Synaptic computation. *Nature* **431**, 796–803.

Aroniadou-Anderjaska V, Zhou F-M, Priest CA, Ennis M & Shipley MT (2000). Tonic and synaptically evoked presynaptic inhibition of sensory input to the rat olfactory bulb via $GABA_B$ heteroreceptors. *J Neurophysiol* **84**, 1194–1203.

Betz WJ (1970). Depression of transmitter release at the neuromuscular junction of the frog. *J Physiol* **206**, 629–644.

Bolding KA & Franks KM (2017). Complementary codes for odor identity and intensity in olfactory cortex. *Elife* **6**, e22630.

Brecht M & Sakmann B (2002). Dynamic representation of whisker deflection by synaptic potentials in spiny stellate and pyramidal cells in the barrels and septa of layer 4 rat somatosensory cortex. *J Physiol* **543**, 49–70.

Carey RM, Verhagen JV, Wesson DW, Pírez N & Wachowiak M (2009). Temporal structure of receptor neuron input to the olfactory bulb imaged in behaving rats. *J Neurophysiol* **101**, 1073–1088.

Carey RM & Wachowiak M (2011). Effect of sniffing on the temporal structure of mitral/tufted cell output from the olfactory bulb. *J Neurosci* **31**, 10615–10526.

Carlson GC, Shipley MT & Keller A (2000). Long-lasting depolarizations in mitral cells of the rat olfactory bulb. *J Neurosci* **20**, 2011–2021.

Chanda S & Xu-Friedman MA (2010). A low-affinity antagonist reveals saturation and desensitization in mature synapses in the auditory brain stem. *J Neurophysiol* **103**, 1915–1926.

Chen WR & Shepherd GM (2005). The olfactory glomerulus: a cortical module with specific functions. *J Neurocytol* **34**, 353–360.

De Saint Jan D, Hirnet D, Westbrook GL & Charpak S (2009). External tufted cells drive the output of olfactory bulb glomeruli. *J Neurosci* **29**, 2043–2052.

De Saint Jan D & Westbrook GL (2007). Disynaptic amplification of metabotropic glutamate receptor 1 responses in the olfactory bulb. *J Neurosci* **27**, 132–140.

Dittman JS, Kreitzer AC & Regehr WG (2000). Interplay between facilitation, depression, and residual calcium at three presynaptic terminals. *J Neurosci* **20**, 1374–1385.

Duchamp-Viret P, Chaput MA & Duchamp A (1999). Odor response properties of rat olfactory receptor neurons. *Science* **284**, 2171–2174.

Elmqvist D & Quastel DM (1965). A quantitative study of end-plate potentials in isolated human muscle. *J Physiol* **178**, 505–529.

Ennis M, Zhou F-M, Ciombor KJ, Aroniadou-Anderjaska V, Hayar A, Borrelli E, Zimmer LA, Margolis F & Shipley MT (2001). Dopamine D2 receptor-mediated presynaptic inhibition of olfactory nerve terminals. *J Neurophysiol* **86**, 2986–2997.

Foster KA, Kreitzer AC & Regehr WG (2002). Interaction of postsynaptic receptor saturation with presynaptic mechanisms produces a reliable synapse. *Neuron* **36**, 1115–1126.

Fukunaga I, Berning M, Kollo M, Schmaltz A & Schaefer AT (2012). Two distinct channels of olfactory bulb output. *Neuron* **75**, 320–329.

Giraudet P, Berthommier F & Chaput M (2002). Mitral cell temporal response patterns evoked by odor mixtures in the rat olfactory bulb. *J Neurophysiol* **88**, 829–838.

Gire DH, Franks KM, Zak JD, Tanaka KF, Whitesell JD, Mulligan AA, Hen R & Schoppa NE (2012). Mitral cells in the olfactory bulb are mainly excited through a multistep signaling path. *J Neurosci* **32**, 2964–2975.

Gire DH & Schoppa NE (2009). Control of on/off glomerular signaling by a local GABAergic microcircuit in the olfactory bulb. *J Neurosci* **29**, 13454–13464.

Hayar A, Shipley MT & Ennis M (2005). Olfactory bulb external tufted cells are synchronized by multiple intraglomerular mechanisms. *J Neurosci* **25**, 8197–8208.

Igarashi KM, Ieki N, An M, Yamaguchi Y, Nagayama S, Kobayakawa K, Kobayakawa R, Tanifuji M, Sakano H, Chen WR & Mori K (2012). Parallel mitral and tufted cell pathways route distinct odor information to different targets in the olfactory cortex. *J Neurosci* **32**, 7970–7985.

Julius D & Katz LC (2004). A Nobel for smell. *Cell* **119**, 747–752.

Kikuta S, Fletcher ML, Homma R, Yamasoba T & Nagayama S (2013). Odorant response properties of individual neurons in an olfactory glomerular module. *Neuron* **77**, 1122–1135.

Kushmerick C, Renden R & von Gersdorff H (2006). Physiological temperatures reduce the rate of vesicle pool depletion and short-term depression via an acceleration of vesicle recruitment. *J Neurosci* **26**, 1366–1377.

Leng G, Hashimoto H, Tsuji C, Sabatier N & Ludwig M (2014). Discharge patterning in rat olfactory bulb mitral cells in vivo. *Physiol Rep* **2**, e12021.

Liley AW & North KA (1953). An electrical investigation of effects of repetitive stimulation on mammalian neuromuscular junction. *J Neurophysiol* **16**, 509–527.

Lu H-W & Trussell LO (2016). Spontaneous activity defines effective convergence ratios in an inhibitory circuit. *J Neurosci* **36**, 3268–3280.

Lynch JW & Barry PH (1989). Action potentials initiated by single channels opening in a small neuron (rat olfactory receptor). *Biophys J* **55**, 755–768.

Maher BJ & Westbrook GL (2008). Co-transmission of dopamine and GABA in periglomerular cells. *J Neurophysiol* **99**, 1559–1564.

Mennerick S & Matthews G (1996). Ultrafast exocytosis elicited by calcium current in synaptic terminals of retinal bipolar neurons. *Neuron* **17**, 1241–1249.

Murphy GJ, Glickfeld LL, Balsen Z & Isaacson JS (2004). Sensory neuron signaling to the brain: properties of transmitter release from olfactory nerve terminals. *J Neurosci* **24**, 3023–3030.

Nagayama S, Takahashi YK, Yoshihara Y & Mori K (2004). Mitral and tufted cells differ in the decoding manner of odor maps in the rat olfactory bulb. *J Neurophysiol* **91**, 2532–2540.

Najac M, De Saint Jan D, Reguero L, Grandes P & Charpak S (2011). Monosynaptic and polysynaptic feed-forward inputs to mitral cells from olfactory sensory neurons. *J Neurosci* **31**, 8722–8729.

Neher E (2015). Merits and limitations of vesicle pool models in view of heterogeneous populations of synaptic vesicles. *Neuron* **87**, 1131–1142.

Nickell WT, Behbehani MM & Shipley MT (1994). Evidence for $GABA_B$-mediated inhibition of transmission from the olfactory nerve to mitral cells in the rat olfactory bulb. *Brain Res Bull* **35**, 119–123.

Regehr WG (2012). Short-term presynaptic plasticity. *Cold Spring Harb Perspect Biol* **4**, a005702.

Rospars J-P, Lánský P, Duchamp A & Duchamp-Viret P (2003). Relation between stimulus and response in frog olfactory receptor neurons in vivo. *Eur J Neurosci* **18**, 1135–1154.

Rudolph S, Tsai MC, von Gersdorff H, Wadiche JI (2015). The ubiquitous nature of multivesicular release. *Trends Neurosci* **38**,428–438.

Sakaba T & Neher E (2001). Calmodulin mediates rapid recruitment of fast-releasing synaptic vesicles at a calyx-type synapse. *Neuron* **32**, 1119–1131.

Saviane C & Silver RA (2006). Fast vesicle reloading and a large pool sustain high bandwidth transmission at a central synapse. *Nature* **439**, 983–987.

Schneggenburger R, Meyer AC & Neher E (1999). Released fraction and total size of a pool of immediately available transmitter quanta at a calyx synapse. *Neuron* **23**, 399–409.

Schneggenburger R, Sakaba T & Neher E (2002). Vesicle pools and short-term synaptic depression: lessons from a large synapse. *Trends Neurosci* **25**, 206–212.

Schoppa NE & Westbrook GL (2001). Glomerulus-specific synchronization of mitral cells in the olfactory bulb. *Neuron* **31**, 639–651.
Shao Z, Puche AC, Kiyokage E, Szabo G & Shipley MT (2009). Two GABAergic intraglomerular circuits differentially regulate tonic and phasic presynaptic inhibition of olfactory nerve terminals. *J Neurophysiol* **101**, 1988–2001.
Sicard G (1986). Electrophysiological recordings from olfactory receptor cells in adult mice. *Brain Res* **397**, 405–408.
Silver RA, Lubke J, Sakmann B & Feldmeyer D (2003). High-probability uniquantal transmission at excitatory synapses in barrel cortex. *Science* **302**, 1981–1984.
Silver RA, Momiyama A & Cull-Candy SG (1998). Locus of frequency-dependent depression identified with multiple-probability fluctuation analysis at rat climbing fibre-Purkinje cell synapses. *J Physiol* **510**, 881–902.
Tan J, Savigner A, Ma M & Luo M (2010). Odor information processing by the olfactory bulb analyzed in gene-targeted mice. *Neuron* **65**, 912–926.
Taschenberger H, Woehler A & Neher E (2016). Superpriming of synaptic vesicles as a common basis for intersynapse variability and modulation of synaptic strength. *Proc Natl Acad Sci USA* **113**, E4548–E4557.
Thanawala MS & Regehr WG (2016). Determining synaptic parameters using high-frequency activation. *J Neurosci Methods* **264**, 136–152.
Trussell LO, Zhang S & Raman IM (1993). Desensitization of AMPA receptors upon multiquantal neurotransmitter release. *Neuron* **10**, 1185–1196.
Turecek J, Jackman SL & Regehr WG (2016). Synaptic specializations support frequency-independent Purkinje cell output from the cerebellar cortex. *Cell Rep* **17**, 3256–3268.
Vaaga CE & Westbrook GL (2016). Parallel processing of afferent olfactory sensory information. *J Physiol* **594**, 6715–6732.
Vaaga CE, Yorgason JT, Williams JT & Westbrook GL (2017). Presynaptic gain control by endogenous cotransmission of dopamine and GABA in the olfactory bulb. *J Neurophysiol* **117**, 1163–1170.
von Gersdorff H & Borst JGG (2002). Short-term plasticity at the calyx of Held. *Nat Rev Neurosci* **3**, 53–64.
Wachowiak M, McGann JP, Heyward PM, Shao Z, Puche AC & Shipley MT (2005). Inhibition of olfactory receptor neuron input to olfactory bulb glomeruli mediated by suppression of presynaptic calcium influx. *J Neurophysiol* **94**, 2700–2712.
Wadiche JI & Jahr CE (2001). Multivesicular release at climbing fiber-Purkinje cell synapses. *Neuron* **32**, 301–313.
Wang LY & Kaczmarek LK (1998). High-frequency firing helps replenish the readily releasable pool of synaptic vesicles. *Nature* **394**, 384–388.
Welker WI (1964). Analysis of sniffing in the albino rat. *Behavior* **22**, 223–244.
Wong AYC, Graham BP, Billups B & Forsythe ID (2003). Distinguishing between presynaptic and postsynaptic mechanisms of short-term depression during action potential trains. *J Neurosci* **23**, 4868–4877.
Youngentob SL, Mozell MM, Sheehe PR & Hornung DE (1987). A quantitative analysis of sniffing strategies in rats performing odor discrimination tasks. *Physiol Behav* **41**, 59–69.

Additional information

Competing interests

The authors declare no competing interests, financial or otherwise.

Author contributions

The work was carried out in the Westbrook Laboratory at the Vollum Institute at Oregon Health and Science University. C.E.V. and G.L.W. designed and conceived of the work. C.E.V. performed the experiments and analysed the data. C.E.V. and G.L.W. drafted and revised the manuscript. Both C.E.V. and G.L.W. approve the final version of the manuscript, and agree to be accountable for all aspects of the work. All persons designated as authors qualify for authorship, and all persons that qualify for authorship are listed.

Funding

This work was supported by NS26494 (G.L.W.; NIH, NINDS), National Science Foundation Graduate Research Fellowship DGE 0925180 (C.E.V.), and a LaCroute Neurobiology of Disease fellowship (C.E.V.).

Acknowledgements

We thank Dr Henrique von Gersdorff and members of the Westbrook lab for helpful comments on this manuscript.